Perspectives on the observation of clusters of galaxies in X-ray band with SAX (X-ray Astronomy Satellite) (*)

C. SIGISMONDI

Dipartimento di Fisica and ICRA, International Center for Relativistic Astrophysics
Università di Roma I "La Sapienza" - P.le A. Moro 2, I-00185 Roma, Italy

(ricevuto il 30 Luglio 1996)

Summary. — By observing clusters of galaxies in the X-ray band it is possible to measure the total gravitational mass (dark matter included) perhaps more precisely than the same measure obtained from optical data. How to make this measure with SAX (X-ray Astronomy Satellite) is the aim of this work. The response of SAX X-ray telescopes with extended spherically symmetric sources is studied in order to set an image-deconvolution procedure. Realistic Monte Carlo simulations of observations of isothermal and polytropic X-ray clusters of galaxies have been examined.

PACS 95.55.Ka – X- and γ-ray telescopes and instrumentation.
PACS 95.75.Mn – Image processing.
PACS 98.65 – Galaxy groups, clusters and superclusters; large scale structure of the Universe.
PACS 95.75.Fg – Spectroscopy and spectrophotometry.
PACS 01.30.Cc – Conference proceedings.

1. – Introduction

SAX, X-ray Astronomy Satellite [1-3], was launched on 29th April 1996 on the "Atlas Centauri" vector from Cape Canaveral base. On board of this satellite there are four X-ray grazing-incidence telescopes with Gas Scintillation Proportional Counter (GSPC) as detectors.

The response of those systems interacting with extended X-ray sources like clusters of galaxies, has been studied, in order to set an image-deconvolution procedure and to define the observational program of this mission.

The intracluster gas is responsible for X-ray emission; in sect. **2** the X-ray emission from clusters of galaxies and some goals of X-ray spatially resolved spectroscopy with clusters of galaxies are presented.

(*) Paper presented at the Fourth Italian-Korean Meeting on Relativistic Astrophysics, Rome-Gran Sasso-Pescara, July 9-15, 1995.

In sect. **3** and **4** two models of gas distribution in cluster potential are discussed: the isothermal and the polytropic one.

In sect. **5** the emission model of this gas and the X-ray sky background model are presented; all those models have been chosen for simulations, based on the Monte Carlo method, of X-ray clusters of galaxies observations.

In those simulations a photon list from the cluster and the X-ray sky background is processed by a ray-tracing Monte Carlo program in which the complex geometry, the physics of the grazing incidence of X-ray SAX telescopes and the physics of GSPC detectors are represented (sect. **6**).

In sect. **7** the processes that are the main responsible for the image blurring are shown.

In sect. **8** an image-deconvolution procedure (only for spherical symmetry) is presented.

Finally, in sect. **9** the temperature profiles and iron abundance profiles measured from simulated observation of four X-ray clusters of galaxies are presented: isothermal (near and far) and polytropic (near and far).

2. – X-ray emission from clusters of galaxies: the spatially resolved spectroscopy within the hydrostatic model

The clusters of galaxies are bright sources of X-ray (see [4] for a complete review), their flux is about $10^{45}\,\mathrm{erg/s}$, and their X-ray luminosity is not due only to the contributions of single galaxies. They are filled by hot gas at temperature $T \approx 10^8\,\mathrm{K}$ and density $n \approx 10^{-3}\ \mathrm{atoms \cdot cm^{-3}}$. This intracluster gas is considered a good tracer of the cluster gravitational potential because its distribution maps continously the whole mass distribution (visible and dark matter). This gas radiates in X-ray band because of the thermal bremsstrahlung, responsible for the continuum features in the spectrum (dominant at $T > 3\ \mathrm{keV} \approx 3.4 \cdot 10^7\,\mathrm{K}$ with respect to lines emission), and because of the particular atomic transitions of heavy ions such as O, Si, Fe, Mg, C, Ni; the main spectral feature is a blend of lines of iron and nickel (hydrogen and helium-like) called 7-keV Fe line, [4, 5]. The intracluster gas may be considered optically thin and in hydrostatic equilibrium; assuming the distribution spherically symmetric,

$$\frac{1}{\varrho_{\mathrm{gas}}} \cdot \frac{\mathrm{d}P}{\mathrm{d}r} = -\frac{GM(<r)}{r^2} = -\frac{\mathrm{d}\phi}{\mathrm{d}r} \tag{1}$$

and the perfect-gas state equation,

$$P = \frac{\varrho_{\mathrm{gas}} KT}{\mu m_{\mathrm{p}}}\,, \tag{2}$$

where G is the gravitational constant, K is the Boltzmann constant, μ is the mean atomic weight of the gas, m_{p} is the proton mass; it is possible to derive the well-known formula that obtains total gravitational binding mass $M(<r)$ contained in an r-radius

sphere from the logarithmic derivatives of temperature and density of intracluster gas [6],

$$M_{\mathrm{tot}}(r) = -\frac{KT}{\mu m_{\mathrm{p}} G}\cdot\left(\frac{\mathrm{d}\ln \varrho_{\mathrm{gas}}(r)}{\mathrm{d}\ln r} + \frac{\mathrm{d}\ln T(r)}{\mathrm{d}\ln r}\right)\cdot r\,, \tag{3}$$

where $T(r)$ and $\varrho(r)$ are temperature and density as functions of radius.

The measure of $T(r)$ and $\varrho(r)$ is possible by performing spatially resolved spectroscopy.

The measure of the total gravitational mass, including dark matter, is also realisable from optical data: using the dispersion of velocities of galaxies and the hypotesis of hydrostatic equilibrium of galaxies and the hypotesis of complete virialization of the cluster. This latter hypotesis would be satisfied if the galaxies were the only "mass carriers" of the cluster, but the existence of intracluster gas requires the additional hypotesis that makes the X-ray–based measure more simple; moreover, in order to map the cluster gravitational potential the galaxies distribution is not as continuous and diffuse as the gas one.

By measuring eventual space gradients of abundance of heavy ions (with spatially resolved spectroscopy) it is possible to test some hypotesis on their origin and on the origin of the whole gas, which sometimes is so much to make the simple hypotesis of its galactic origin unrealistic [4].

3. – The isothermal model for intracluster gas distribution

The galaxies in the cluster may be also well represented from a perfect-gas equation:

$$P = \varrho_{\mathrm{gal}}\sigma_r^2 \tag{4}$$

and in spherical symmetry their equation of dynamics is

$$\frac{\mathrm{d}\ln \varrho_{\mathrm{gal}}}{\mathrm{d}r} = -\frac{1}{\sigma_r^2}\frac{\mathrm{d}\phi}{\mathrm{d}r}\,, \tag{5}$$

where the temperature of the "gas" of galaxies is the dispersion of the velocity on the line of sight.

i) In order to obtain the isothermal model for intracluster gas distribution, assuming T and σ_r^2 constants with respect to the radius (isothermality); ii) considering negligible the intracluster gas contribution to the gravitational potential [7-9] and iii) that this potential is derivable from the distribution of galaxies that follows the whole mass distribution [10, 11], eq. (1) for the intracluster gas can also be written as

$$\frac{\mathrm{d}\ln \varrho_{\mathrm{gas}}}{\mathrm{d}r} = -\frac{\mu m_{\mathrm{p}}}{kT}\frac{\mathrm{d}\phi}{\mathrm{d}r}\,. \tag{6}$$

If T and σ_r^2 are constants with respect to the radius, the solutions of (5) and (6) are in this relation:

$$\varrho_{\mathrm{gas}}(r) = \varrho_{\mathrm{gal}}(r)^{\frac{\sigma_r^2\mu m_{\mathrm{p}}}{KT}}, \tag{7}$$

where the ratio at exponent is named usually β-factor, and it is the ratio between the energy of galaxies per unity of mass and that of the gas. The King formula [12] describes the density of the self-gravitating spherically symmetric isothermal distribution of galaxies,

$$\varrho_{\mathrm{gal}}(r) = \varrho_{\mathrm{central}}\left[1 + \left(\frac{r}{r_{\mathrm{core}}}\right)^2\right]^{-3/2}, \tag{8}$$

the core radius being where the projected density is exactly $1/2$ of the central density; thus assuming the temperature of gas isothermal, inserting (8) in (7), the equation for the density of an isothermal intracluster gas is obtained.

4. – The polytropic model of intracluster gas distribution

Another hypotesis (with respect to the hypothesis i) of sect. **3**, being also valid the other two hypotheses) is that the relation between state parameters is polytropic,

$$TP^{\frac{1-n}{n}} = \mathrm{const}\,. \tag{9}$$

This additional hypotesis must be intended only in the sense of initial entropy profile of intracluster gas and not as stating that the gas is subjected to polytropic thermodynamical transformations, because those transformations are all quite adiabatic. Here the polytropic index n does not depend on the ratio of specific heats $n_{\text{specific heats}} = \frac{C_{\mathrm{Pol}} - C_{P=\mathrm{const}}}{C_{\mathrm{Pol}} - C_{V=\mathrm{const}}}$. It is possible to have a polytropic index $n = 1$ (isothermal profile) and an $n_{\text{specific heats}} = 5/3$ that is the ratio of specific heats in the adiabatic monoatomic-gas case [13].

Taking the logarithmic derivative of eq. (9) with respect to the radius, taking the pressure gradient from the spherically symmetric hydrostatic condition (6), the pressure expression from the prefect-gas state equation (2), one obtains

$$\frac{\mathrm{d}T}{\mathrm{d}r} = \left(\frac{1-n}{n}\right)\frac{\mu m_{\mathrm{p}}}{K}\,\frac{\mathrm{d}\phi}{\mathrm{d}r}\,. \tag{10}$$

Integrating this equation, choosing $\mu = 1$, $\sigma_r = 1000$ km/s, and taking the potential gradient from (5) one finally obtains

$$T(r) = T(0) - 15.5\ \mathrm{keV}\left(\frac{n-1}{n}\right)\ln\left[1 + \left(\frac{r}{r_{\mathrm{core}}}\right)^2\right] \tag{11}$$

and the corresponding formula for the density obtained from the polytropic equation in the form

$$\frac{\varrho(r)}{\varrho(0)} = \left(\frac{T(r)}{T(0)}\right)^{\frac{1}{n-1}}. \tag{12}$$

5. – X-ray emission model and X-ray sky background model adopted for Monte Carlo simulations of source-photon list

With respect to the energy spectrum of X-ray emission the Mewe code has been used [14], in which both the continuum features of the spectrum and those of the lines are represented. For the continuum features the emissivity per unity of volume, frequency and time can be written as [5]

$$\varepsilon_{\text{free free}}(\nu) = 6.8\cdot 10^{-38}\sqrt{T}\exp\left[\frac{-h\nu}{KT}\right] g_{\text{free free}}\, n_{\text{i}}(r)\cdot n_{\text{e}}(r)\cdot Z^2\,\frac{\text{erg}}{\text{Hz}\cdot\text{cm}^3\cdot\text{s}}\,, \tag{13}$$

where $g_{\text{free free}}$ is the Gaunt factor, that is about 1.2 within 20% of variation in our physical conditions; $n_{\text{e}}(r)$ and $n_{\text{i}}(r)$ are the number of electrons and positive ions per unit of volume; $h\nu = E$ is the photon energy; T is the gas temperature in Kelvin degrees (that is the same for the ions and for the electrons [4, 15]); if the gas were pure hydrogen, $Z = 1$ and $n_{\text{e}} = n_{\text{i}}$.

At those photons the photons from X-ray cosmic background have been adjointed; this background is isotropical and its energy spectrum in the 1–10 keV band is quite a power law [16]:

$$F(E) = 5.6\cdot\frac{1}{E}\cdot\left(\frac{E}{3\ \text{keV}}\right)^{-0.29}\cdot\exp\left[\frac{-E}{40\ \text{keV}}\right]\frac{\text{photons}}{\text{keV}\cdot\text{cm}^2\cdot\text{s}\cdot\text{sterrad}}\,. \tag{14}$$

The Monte Carlo method is a procedure that allows to obtain a data set $\{x_i\}$ with a definite distribution function $f(x_i)$ in the range $[x_{\min}, x_{\max}]$ starting from a set of random numbers $\{r_i\}$ uniformly distributed in $[0, 1]$ range. It is necessary to solve analytically or numerically the following equation:

$$r_i = \frac{\int_{x_{\min}}^{x_i} f(y)\ \text{d}y}{\int_{x_{\min}}^{x_{\max}} f(y)\ \text{d}y} \tag{15}$$

with respect to the unknown x_i.

The function $f(x_i)$ has been the Mewe code [14] to obtain a set of photon energy correctly distributed, or eqs. (7) or (12) to obtain a spatial distribution of photons compatible with the density law for the isothermal or polytropic model, or eq. (16) in order to represent the instrumental background, or the cross-section of grazing incidence of an X-ray photon over a gold surface with some micro-roughness, or the photon cross-section of absorption in the detector window, or, finally, the photon cross-section of absorption in the xenon atmosphere.

6. – The simulations of observations with SAX X-ray telescopes using a ray-tracing program

SAX satellite has four X-ray telescopes called concentrators/spectrometers (C/S) [1, 2]. Every C/S is composed by 30 confocal and coaxial gold mirrors embedded into each other [17]; each mirror is a conical approximation of a Wolter-1 configuration:

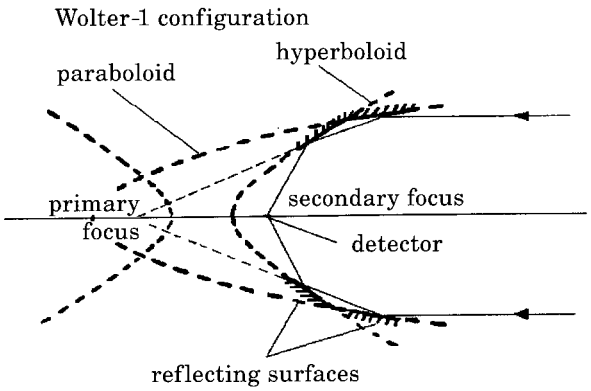

Fig. 1. – Wolter-1 configuration of the optics of the concentrators/spectrometers (see sect. **6**).

paraboloid (first reflection) and hyperboloid (second reflection)-mirror [18-20], as shown in fig. 1.

The name "concentrator" means that it is able only to concentrate the radiation and not to focus it (as it may be for the Wolter-1 configuration, but only in a small region). The "concentration power" is good in a wider field-of-view region with respect to Wolter-1 focus power; obviously, the spatial resolution of a C/S optic is lower than that of Wolter-1: one arcminute with respect to some arcseconds.

Another advantage of the conical approximation with respect to the Wolter-1 is the small weight of the structure, because even small geometrical deformations are not able to lose the concentration power.

The C/S have Gas Scintillation Proportional Counters (GSPC) as detectors [21]; three of those C/S GSPC are position-sensitive in the 1–10 keV energy band (Medium Energy C/S, MECS), the last is sensitive in the 0.1–10 keV band (Low Energy C/S, LECS). This work is limited to 1–10 keV MECS energy band.

In the ray-tracing program each interaction of the X-ray photon with the mirror surface or with the window of GSPC detector or during its absorption in the xenon atmosphere of GSPC is treated as stochastic process with the three relative event cross-sections. Each of them in a Monte Carlo procedure (eq. (14)).

For the simulation of the instrumental background the ultra-conservative estimation of the number of events

$$N(E) = 0.002 \ \frac{\text{events}}{\text{keV}\cdot\text{cm}^2\cdot\text{s}} \tag{16}$$

has been used.

The instrumental parameters such as "concentration power", detection efficiency, micro-roughness scattering, etc., limiting the research to point-like sources, have been studied with a ray-tracing program [22] in wich the complex geometry, the grazing incidence over rough surfaces [23] and the detector physics are represented.

The utilization of this ray-tracing program with extended sources is the particularity of this work: every photon in the source list (included sky X-ray background photons) is treated as a single point-like source.

7. – Images with SAX concentrators/spectrometers: the causes of the blurring

There are four kinds of process that cause the blurring of the images [24]. They are:

1) The concentration effect, due to unability to focus of the optics.

2) The diffusion effect, or scattering from micro-roughness (some angstroms) of the mirrors gold surface.

3) The spatial resolution of the detector, due to the Poissonian error associated to the scintillation counts.

4) The "stray-lights effect", due to the photons that do not have the two canonical reflections on the mirrors [25].

The concentration effect is the most important one, and its "correction" is explained in sect. **8**.

The diffusion effect is more efficient at high energies, because the micro-roughness is more important as the wavelength of the photon decreases and becomes as small as the micro-roughness.

The spatial resolution of the detector occurs in the revelation process, in counting UV scintillations, that are directly proportional to the photon original energy [21]. Both the determination of the photon energy and the photon position in the focal plane are subjected to Poissonian statistical error [27]. Because of it, N counts have an error of about $\sqrt{N}$. Thus even a two-reflections photon may be detected in a zone different from that corresponding to the original zone of the source, and this blurring effect, that is dependent only on the photon energy, occurs inside the detector and is efficient at low energies:

$$\sigma(E) = \sigma(E_0)\cdot\left(\frac{E}{E_0}\right)^{0.5}, \tag{17}$$

where σ may represent either the spatial shift, or the energy shift in detection processes.

The stray-lights effect depends on the telescopes geometry and also on the X-ray photon energy and is more efficient at low energies. It is due to the photons that have only one reflection over the surface of the mirrors. A "canonical path" for a photon is the one in which there are two reflections: one over the paraboloid and one over the hyperboloid (their conical approximations). The grazing-incidence angles must be lower than the critical angle that is inversely proportional to the photon energy, and for gold is $\theta_{\mathrm{crit}} = \frac{3.4^\circ}{E(\mathrm{keV})}$ [28], thus the one-reflection paths are possible only for low-energy photons (because of their big grazing-incidence angle, sufficient to skip the first or the second mirror): those photons fall into detector zones that do not correspond to the original sky zone of birth, while the two-reflection photons fall onto a zone quite corresponding to the original sky zone.

8. – The "rings method" of images deconvolution of spherical clusters

Working with extended sources, the spatial resolution of SAX C/S in 1–10 keV energy band has been chosen as 2 arcminutes: within this value two equal point-like

sources of energy in the range 1–10 keV are well resolved in the whole field of view, considering either the optics either the detector effects [24]. Assuming the sources on-axis with spherical symmetry, the corresponding two-dimensional images are cilindrycal symmetric, *id est* annular symmetric.

With those symmetries it is natural to define the effective area of the telescopes optics as the ratio between the number of photons arrived (not yet detected) at a ring of the detector window and those that were in a "sky ring" source multiplied by geometrical exposed area of mirrors:

$$A_{\mathrm{eff}}(E,\theta) = A_{\mathrm{geom}}(\theta)\cdot N_{\text{annular counts}}(E,\theta)/N_{\text{sky ring source}}(E,\theta), \tag{18}$$

where θ now is the mean angular off-axis radius of the ring and E is the photon energy.

This choice of effective area corresponds to considering that the concentration effect, due only to the geometry of the optics, may blur the image of an original sky ring source, but its effect is limited only within the corresponding detector ring.

This effective area is not yet ready for applications in data reduction, it is to be corrected for the diffusion effect and for the effect of the spatial resolution of the detector, the last effect of the stray lights being negligible.

Usually, the effective area of the optics, the transmission function of the detector window and the quantum efficiency of the xenon atmosphere are considered as three separate parameters [27], but it is convenient to mix the traditional definitions of those three parameters in order to take into account the diffusion effect and the spatial resolution of the detector.

It is observed that the former effect (diffusion) acts on high-energy photons, and the latter (spatial resolution of the detector) on the low-energy ones so that the whole energy spectrum in a 2-arcminutes ring is conserved in shape (but not in normalization) with respect to the energy spectrum of all the photons detected from the whole detector.

This observation has suggested the use of a sligtly different definition of "rings effective area":

$$A_{\mathrm{eff}}(E,\theta) = A_{\mathrm{geom}}(\theta)\cdot N_{\text{counts over all surface of detector window}}(E,\theta)/N_{\text{sky ring source}}(E,\theta). \tag{19}$$

9. – Conclusions: the application of "rings method" to the simulations of isothermal and polytropic clusters

With the definition (19) of the effective area it should be possible to derive the original energy spectrum in shape, but not in normalization, from the simulated data. This is the reason why only the temperature and the iron abundance are studied, but not yet the density of the intracluster gas models chosen for those simulations of observation.

The measure of the temperature T and of the iron abundance A_{Fe} from the energy spectrum data is possibile by studying only the form of the spectrum: T is measurable from the exponential cut-off of the continuum feature of the spectrum (see the formula (13)), while A_{Fe} is derivable from the 7 keV iron blend equivalent width (see [27] for a complete review of data reduction in X-ray Astronomy).

It is necessary to emphasize that while the isothermal models have the same temperature and iron abundance in each ring of source, and only the projected density

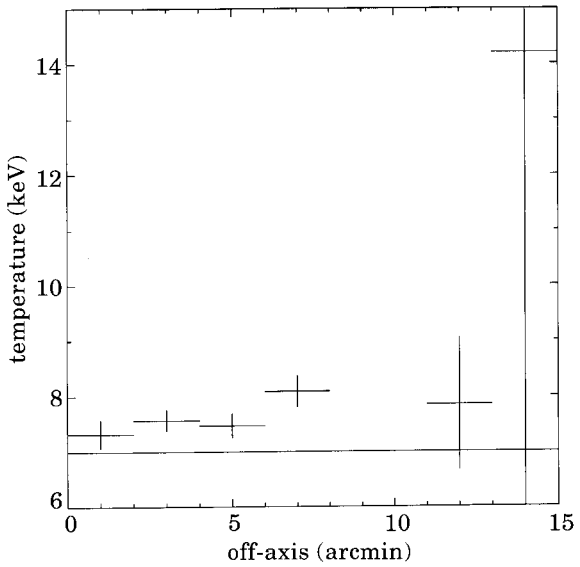

Fig. 2. – Temperature of near isothermal cluster; the temperature of the model is $T = 7$ keV (continuous line; see sect. **9**).

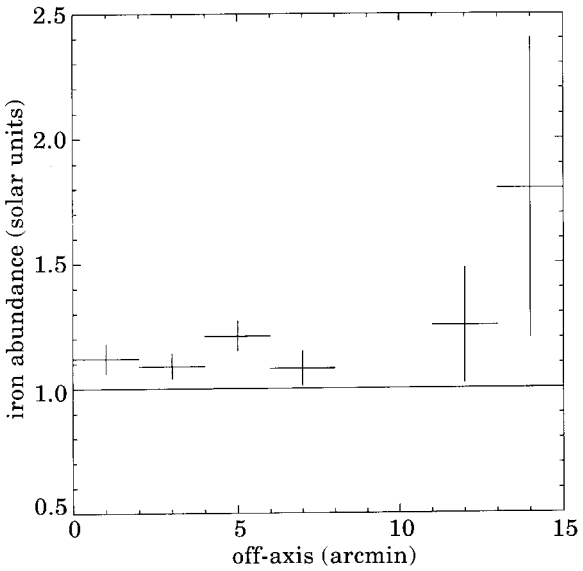

Fig. 3. – Iron abundance of near isothermal cluster measured in solar units; the iron abundance of the model is the solar one (continuous line; see sect. **9**).

changes, in the polytropic ones the temperature is not constant with respect to the three-dimensional radius, but in the projected distribution the contribution of the photons of the outer shells is negligible because of the power law three-dimensional

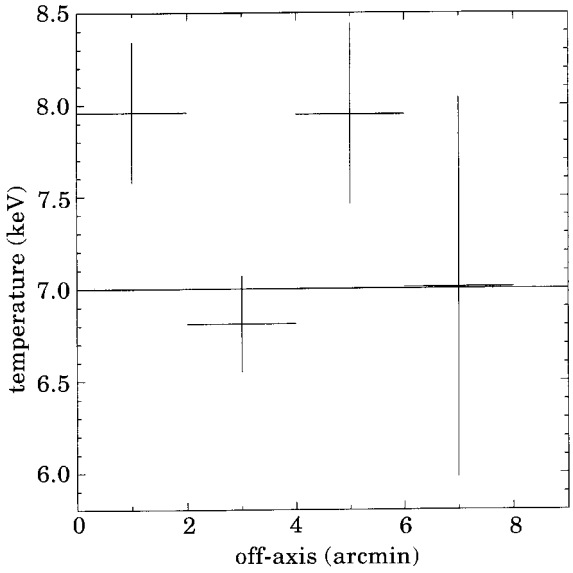

Fig. 4. – Temperature of far isothermal cluster; the temperature of the model is $T = 7$ keV (continuous line; see sect. **9**).

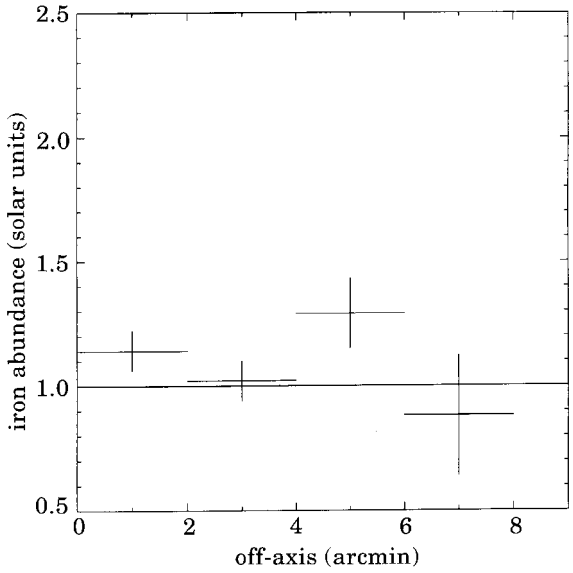

Fig. 5. – Iron abundance of far isothermal cluster measured in solar units; the iron abundance of the model is the solar one (continuous line; see sect. **9**).

density distribution of the intracluster gas (see eqs. (11) and (12)). Thus in each image ring the temperature T has been considered constant and its value has been considered corresponding to the value of T at the mean radius of the ring (that is equal to the

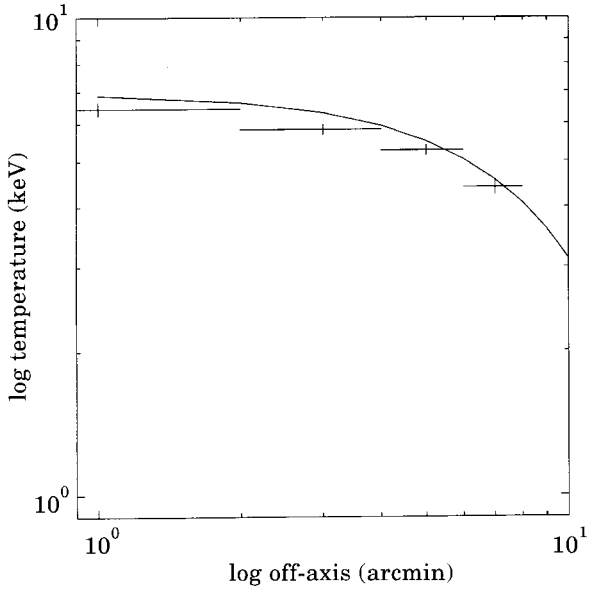

Fig. 6. – Temperature of near polytropic cluster; the temperature of the model is the continuous line (see sect. **9**).

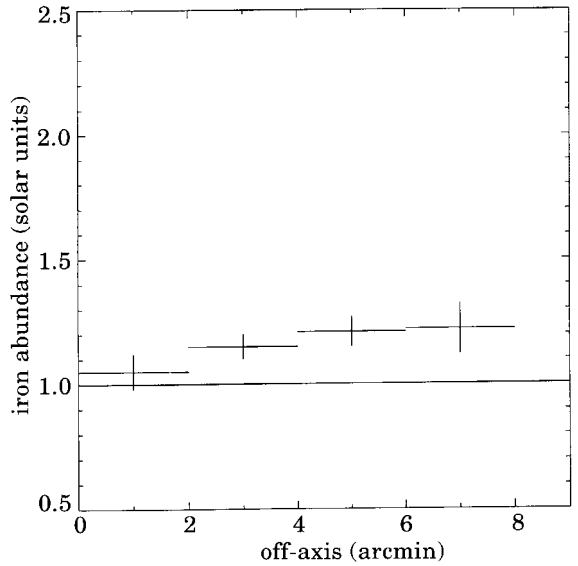

Fig. 7. – Iron abundance of near polytropic cluster measured in solar units; the iron abundance of the model is the solar one (continuous line; see sect. **9**).

three-dimensional radius, having the spherically symmetric source on-axis and with the previous hypotesis of the different three-dimensional shell contribution).

The value of iron abundance has been simulated in all the models equal to

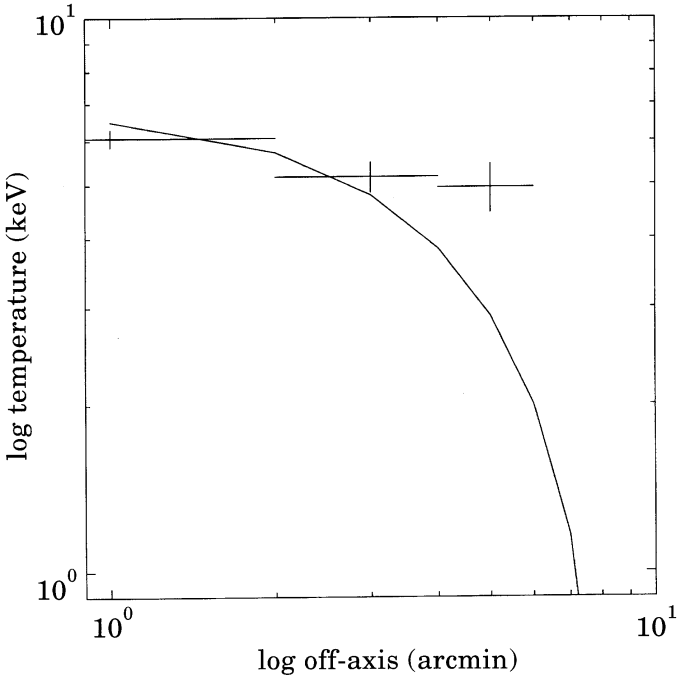

Fig. 8. – Temperature of far polytropic cluster; the temperature of the model is the continuous line (see sect. **9**).

the solar value (in excess with respect to the real value that seems to be about 0.3 times the solar value), constant with radius.

In the simulations of isothermal clusters (see eqs. (7) and (8)), $\beta = 0.7$, $T = 7$ keV, and central gas density $\varrho_{\text{central}} = 4.56 \cdot 10^{-3}$ atoms $\cdot$ cm^{-3}. The core radius is 0.2 Mpc for all the clusters. The simulations have been extended just to $4 \cdot r_{\text{core}}$. The flux in the 0.5–4.5 keV X-ray band of the two isothermal models is about $4 \cdot 10^{44}$ erg/s, and the near one is at 171.9 Mpc of distance, while the far one is at 343.8 Mpc, the intensity detected is scaling with the simple inverse-square law of the distance.

In the simulations of polytropic clusters with respect to spatial distribution of density and temperature of the gas eqs. (11) and (12) for the polytropic model have been used, in order to generate the stochastic photon list for ray-tracing program that simulates the telescopes.

The central temperature $T(0) = 7$ keV, and the central gas density $\varrho_{\text{central}} = 4.56 \cdot 10^{-3}$ atoms $\cdot$ cm^{-3} are equal to those of the isothermal model. The core radius is 0.2 Mpc for all the clusters. The polytropic index $n = 4/3$ in both cases, the simulations have been extended just to $2.25 \cdot r_{\text{core}}$, where the temperature (and, consequently, also the density) vanishes. The flux in the 0.5–4.5 keV X-ray band of the two polytropic models is about 10^{44} erg/s and the near one is at a distance of 85.95 Mpc, while the far one is at 171.9 Mpc, thus the projected radius where T reaches the zero value is about 18 arcminutes for the near one, and 9 arcminutes for the far one.

The intensity detected is scaling with the simple inverse-square law of the distance.

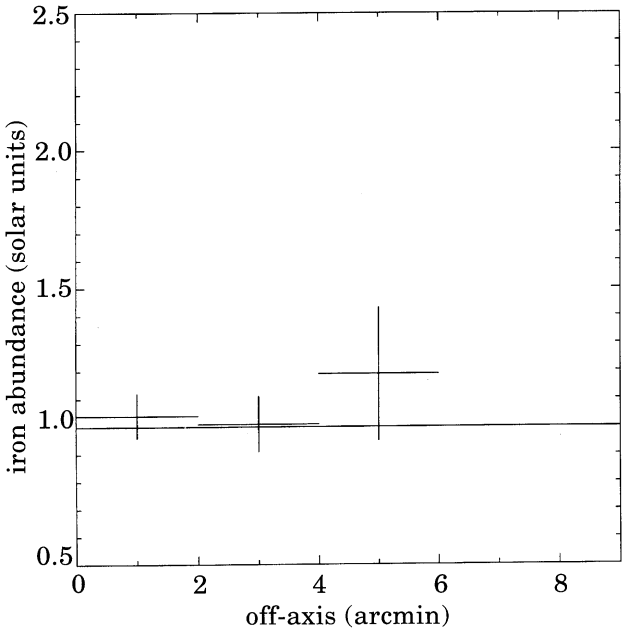

Fig. 9. – Iron abundance of far polytropic cluster measured in solar units; the iron abundance of the model is the solar one (continuous line; see sect. **9**).

In figs. 2-9 the measure of the temperature and the iron abundance in four X-ray clusters of galaxies are shown: isothermal near and far; polytropic near and far, during 120 000 s of observation with one C/S, or, equivalently, 30 000 s of observation with all four C/S.

The clusters near and far have been simulated in order to evaluate the response of the telescopes with a different action of the concentration effect because these two kinds of source are less or more central-condensed; in the X-ray clusters classification [29] they correspond, respectively, to near = nXD (X-ray emission not central-condensed, without central-dominant X-ray galaxy) and far = XD (with central condensation of X-ray brightness surface and central-dominant X-ray galaxy).

The differences noted between the result of this measure of T and A_{Fe} and the true values of T and A_{Fe} utilized in each simulation (see the continous lines in figs. 2-9) are to be considered such as systematical effects (or errors) associated to this procedure. Those systematical effects are able to smooth the possible space gradients of temperature and iron abundance, as is evident from figs. 2-9. They are due principally to the concentration effect of the optics, that are not able to well concentrate the photons of the core region, the denser one, in the corresponding detector zone, so those photons are revealed out of the central ring (disc) of detector, with a “pollution” of the outer rings.

It is remarkable that in previous X-ray Astronomy space missions small or no gradients have been observed in intracluster gas [26, 30-33].

In order to evaluate the possibility for the SAX C/S to perform measures of spatially resolved spectroscopy of extended sources, it needs to “subtract” the systematical error, as defined above, to the measures obtained from the “rings

processed" image. So it is possible to demonstrate that SAX may detect some interesting features as temperature and iron abundance gradients with good experimental relative errors (10 %) in gas of clusters of galaxies [24].

* * *

I am grateful to my thesis advisor Prof. G. C. PEROLA for his guidance and several illuminating discussions.

REFERENCES

[1] PEROLA G. C., *Proceedings of the Workshop on "Non-Thermal and Very High Temperature Phenomena in X-ray Astronomy"*, edited by G. C. PEROLA and M. SALVATI (Istituto Astronomico, Università "La Sapienza", Roma) 1983, p. 175.
[2] SCARSI L., *Astron. Astrophys. Suppl. Ser.*, **97** (1993) 371.
[3] PIRO L., *Nuovo Cimento C*, **16** (1993) 691.
[4] SARAZIN C. L., *X-ray Emission from Clusters of Galaxies* (Cambridge University Press) 1988.
[5] RYBICKI G. B. and LIGHTMAN A. P., *Radiative Processes in Astrophysics* (Wiley-Interscience, New York, N.Y.) 1979.
[6] FABRICANT D., LECAR M. and GORENSTEIN P., *Astrophys. J.*, **241** (1980) 552.
[7] CAVALIERE A. and FUSCO-FEMIANO R., *Astron. Astrophys.*, **49** (1976) 137.
[8] CAVALIERE A. and FUSCO-FEMIANO R., *Astron. Astrophys.*, **70** (1978) 677.
[9] CAVALIERE A. and FUSCO-FEMIANO R., *Astron. Astrophys.*, **100** (1981) 194.
[10] COMBES F. and PFEMINGER D., in *Clusters of Galaxies*, edited by F. DURRET, A. MAZURE and J. TRANH THANH VAN (Editions Frontières, Gif-sur-Yvette) 1994, p. 3.
[11] EVRARD A. E., METZLER C. A. and NAVARRO J. F., *Mass estimates of X-ray clusters* FERMILAB-Pub-95/337-A, 1995.
[12] BINNEY J. and TREMAINE S., *Galactic Dynamics* (Princeton University Press, Princeton) 1987.
[13] FABIAN A. C., in *Hot Thin Plasmas in Astrophysics*, edited by R. PALLAVICINI (Kluwer Academic Publishers, Dordrecht/Boston/London) 1988, p. 293.
[14] MEWE R., GRONENSCHILD E. and VAN DEN OORD G., *Astron. Astrophys. Suppl.*, **62** (1985) 197.
[15] SPITZER L. jr., *Diffuse Matter in Space* (Interscience Publishers, New York, N.Y.) 1968.
[16] TERASAWA N., *Astrophys. J. Lett.*, **378** (1991) L11.
[17] CONTI G., BONELLI G., MATTAINI E., SANTAMBROGIO E., SACCO B., BRAUNINGER H. and BURKERT W. *et al.*, *Lacquer Coated Mandrels for Production of Replicated X-ray Optics Proc. SPIE*, **1140** (1989) 376.
[18] WOLTER H., *Ann. Phys.* (*Leipzig*), **10** (1952) 94.
[19] WOLTER H., *Ann. Phys.* (*Leipzig*), **10** (1952) 286.
[20] GIACCONI R. and ROSSI B., *J. Geophys.*, **65** (1960) 773.
[21] FRASER G. W., *Detectors in Astronomy* (Cambridge University Press) 1989.
[22] CONTI G., MATTAINI E., SANTAMBROGIO E., SACCO B., CUSUMANO G., CITTERIO O., BRAUNINGER H. and BURKERT W., *Engineering Qualification Model of the SAX X-ray Mirror Unit, Technical data and X-ray imaging characteristics*, in *Proceedings of the Workshop "Multilayer and Grazing Incidence X-ray /EUV Optics II", 14-16 July 1993, San Diego, California, Proc. SPIE*, **2011** (1993) 118.
[23] BECKMANN P. and SPIZZICHINO A., *The Scattering of Electromagnetic Waves from Rough Surfaces* (Pergamon, New York, N.Y.) 1963.

[24] SIGISMONDI C., *Prospettive nell'osservazione degli ammassi di galassie nei raggi X con lo strumento a concentratore di SAX*, Thesis, Università di Roma I "La Sapienza", 1994.
[25] GIACCONI R. and GURSKY H., *X-ray Astronomy* (Reidel, Dordrecht) 1974.
[26] BOEHRINGER H., SCHWARZ R. A., BRIEL U. G., VOGES W., EBELING H., HARTNER G. and CRUDDACE R. G., in *Clusters and Superclusters of Galaxies*, edited by A. C. FABIAN (Kluwer Academic Publishers, Dodrecht/Boston/London) 1992, p. 71.
[27] ZOMBECK M. V., in *Hot Thin Plasmas in Astrophysics*, edited by R. PALLAVICINI (Kluwer Academic Publishers, Dordrecht/Boston/London) 1988, p. 65.
[28] ZOMBECK M. V., *Handbook of Space Astronomy and Astrophysics*, 2nd edition (Cambridge University Press, Cambridge) 1990.
[29] JONES C. and FORMAN W., *Ann. Rev. Astron. Astrophys.*, **20** (1992) 547.
[30] JONES C. and FORMAN W. in *Clusters and Superclusters of Galaxies*, edited by A. C. FABIAN (Kluwer Academic Publishers, Dodrecht/Boston/London) 1992, p. 49.
[31] MUSHOTZKY R., in *Clusters and Superclusters of Galaxies*, edited by A. C. FABIAN (Kluwer Academic Publishers, Dodrecht/Boston/London) 1992, p. 91.
[32] YAMASHITA K., in *Clusters of Galaxies*, edited by F. DURRET, A. MAZURE and J. TRANH THANH VAN (Editions Frontières, Gif-sur-Yvette) 1992, p. 153.
[33] IKEBE Y. *et al.*, in *Clusters of Galaxies*, edited by F. DURRET, A. MAZURE and J. TRANH THANH VAN (Editions Frontières, Gif-sur-Yvette) 1994, p. 163.